NASA TECHNICAL NOTE

NASA TN D-7865

NASA TN D-7865

NUMERICAL SOLUTION OF THE HYPERSONIC VISCOUS-SHOCK-LAYER EQUATIONS FOR LAMINAR, TRANSITIONAL, AND TURBULENT FLOWS OF A PERFECT GAS OVER BLUNT AXIALLY SYMMETRIC BODIES

E. C. Anderson and James N. Moss

Langley Research Center
Hampton, Va. 23665

NATIONAL AERONAUTICS AND SPACE ADMINISTRATION • WASHINGTON, D. C. • FEBRUARY 1975

1. Report No.	2. Government Accession No.	3. Recipient's Catalog No.
NASA TN D-7865		

4. Title and Subtitle	5. Report Date
NUMERICAL SOLUTION OF THE HYPERSONIC VISCOUS-SHOCK-LAYER EQUATIONS FOR LAMINAR, TRANSITIONAL, AND TURBULENT FLOWS OF A PERFECT GAS OVER BLUNT AXIALLY SYMMETRIC BODIES	February 1975
	6. Performing Organization Code

7. Author(s)	8. Performing Organization Report No.
E. C. Anderson and James N. Moss	L-9763
	10. Work Unit No.
9. Performing Organization Name and Address	502-27-03-03
NASA Langley Research Center Hampton, Va. 23665	11. Contract or Grant No.
	13. Type of Report and Period Covered
12. Sponsoring Agency Name and Address	Technical Note
National Aeronautics and Space Administration Washington, D.C. 20546	14. Sponsoring Agency Code

15. Supplementary Notes

E. C. Anderson is a research associate with Old Dominion University Research Foundation, Norfolk, Virginia.

16. Abstract

The viscous-shock-layer equations applicable to hypersonic laminar, transitional, and turbulent flows of a perfect gas over two-dimensional plane or axially symmetric blunt bodies are presented. The equations are solved by means of an implicit finite-difference scheme, and the results are compared with a turbulent-boundary-layer analysis. The agreement between the two solution procedures is satisfactory for the region of flow where streamline swallowing effects are negligible. For the downstream regions, where streamline swallowing effects are present, the expected differences in the two solution procedures are evident.

17. Key Words (Suggested by Author(s))	18. Distribution Statement
Shock layer, viscous Perfect-gas flow Laminar Turbulent	Unclassified – Unlimited Subject Category 34 Fluid Mechanics and Heat Transfer

19. Security Classif. (of this report)	20. Security Classif. (of this page)	21. No. of Pages	22. Price*
Unclassified	Unclassified	35	$3.75

*For sale by the National Technical Information Service, Springfield, Virginia 22151

NUMERICAL SOLUTION OF THE HYPERSONIC VISCOUS-SHOCK-LAYER EQUATIONS FOR LAMINAR, TRANSITIONAL, AND TURBULENT FLOWS OF A PERFECT GAS OVER BLUNT AXIALLY SYMMETRIC BODIES

E. C. Anderson* and James N. Moss
Langley Research Center

SUMMARY

The viscous-shock-layer equations for hypersonic laminar, transitional, and turbulent flows of a perfect gas over two-dimensional plane or axially symmetric blunt bodies are developed and presented. The resulting equations are transformed to a shock-body oriented coordinate system and solved by an implicit finite-difference scheme. The eddy viscosity is approximated by a two-layer model which has been used extensively in turbulent-boundary-layer analyses. Methods for defining the boundary-layer-thickness parameters (required in the eddy-viscosity model) which are consistent with boundary-layer theory are presented.

Numerical solutions of the equations of motion for turbulent viscous shock layers are compared with those of a turbulent-boundary-layer analysis which is not corrected for the entropy variation of the inviscid flow outside the boundary layer. The two solution procedures are in good agreement in the region of flow where the effects of streamline swallowing by the boundary layer are negligible. For the downstream regions, where streamline swallowing effects are present, the expected differences in the two solution procedures are evident. However, to establish the accuracy of the downstream solutions, comparisons with a boundary-layer analysis which accounts for the effects of streamline swallowing are necessary.

INTRODUCTION

The nose blunting required to reduce the surface heat-transfer rates to an acceptable level in the stagnation region of a hypersonic vehicle results in strong entropy gradients through the boundary layer in the downstream region. In the stagnation region, the vorticity interaction between the boundary layer and the external inviscid flow must

---

*Research associate, Old Dominion University Research Foundation, Norfolk, Virginia.

be considered in the analysis if the Reynolds number is sufficiently low. Mayne and Adams (ref. 1) present detailed comparisons of a number of boundary-layer analyses with the viscous-shock-layer analysis developed by Davis (ref. 2). The results presented by Mayne and Adams show that the viscous-shock-layer analysis correctly accounts for viscous-inviscid vorticity interaction, streamline swallowing, and viscous-induced pressure effects. Although the viscous-shock-layer analysis was found to be the more accurate solution technique, Mayne and Adams demonstrate that a conventional boundary-layer analysis corrected for streamline swallowing is sufficiently accurate and is computationally more efficient than the viscous-shock-layer analysis. The comparisons presented by Mayne and Adams are restricted to laminar flows of a perfect gas.

As a result of the increased boundary-layer thickness in turbulent flows, the effects of viscous-induced pressure and the strong entropy gradients produced by the bow shock are more pronounced. For turbulent flows, the solution of the viscous-shock-layer equations should provide a substantially more accurate result than would be obtained with a boundary-layer analysis corrected for streamline swallowing without additional corrections to include interaction of the boundary layer with the external inviscid flow.

For flow conditions in which heat transfer from the shock layer by radiation must be considered, the formulation of the viscous-shock-layer equations provides an important simplification. The presence of the radiative heat flux term in both the inviscid and viscous governing equations necessitates an iterative solution procedure of both sets of equations to achieve the required coupling. Since the necessary coupling of the inviscid- and viscous-flow equations is contained within the viscous-shock-layer equations, the solution of this set of governing equations should be more accurate and computationally more efficient than an iterative solution technique which uses a boundary-layer-type analysis. However, applications of the viscous-shock-layer equations to turbulent flows have not been reported. An independent investigation of the viscous-shock-layer equations for turbulent flow has been developed by Eaton and Larson (ref. 3) concurrently with the present study. The results presented by Eaton and Larson are restricted to the thin-shock-layer assumption and to pointed bodies, as a result of their definition for the location of the boundary-layer edge. The present study considers the complete viscous-shock-layer equations for turbulent flow and presents definitions for the boundary-layer thickness and incompressible boundary-layer displacement thickness which are consistent with boundary-layer theory. Both the present study and that of reference 3 are applicable to a perfect gas. Either analysis can, with minor modifications, be applied to equilibrium flows.

It is noted that the boundary-layer-thickness parameters are introduced into the solution by the two-layer eddy-viscosity model used in the present study and would be unnecessary if an invariant-turbulence model were available. The eddy viscosity is approximated by use of the formulation proposed by Cebeci (ref. 4).

Numerical solutions of the viscous-shock-layer equations for turbulent flow are compared with solutions from the boundary-layer analysis developed by Anderson and Lewis (ref. 5). The two solution procedures show acceptable agreement over the portion of the body where the effects of streamline swallowing by the boundary layer are negligible, and the expected differences are obtained in the region far downstream of the nose. The boundary-layer analysis does not account for streamline swallowing.

SYMBOLS

A^+ damping factor (eqs. (23) and (24))

a_0 quantity defined by equation (A9e)

a_1 quantity defined by equation (A10f)

a_2 quantity defined by equation (A10g)

C_f skin-friction coefficient

c_p specific heat at constant pressure

H defined quantity, $h + \frac{u^2}{2}$

H_t total enthalpy, $H + \frac{v^2}{2}$

h specific enthalpy, $h^* / \left(U_\infty^*\right)^2$

j flow index: 0 for plane flow; 1 for axisymmetric flow

k thermal conductivity

k_T eddy thermal conductivity

ℓ mixing length (eq. (21))

M Mach number

N_{Pr} Prandtl number, $\mu^* c_p^* / k^*$

$N_{Pr,T}$	turbulent Prandtl number, $c_p^* \mu_T^* / k_T^*$
N_{Re}	Reynolds number, $\rho_\infty^* U_\infty^* r_n^* / \mu_\infty^*$
n	coordinate measured normal to body, n^* / r_n^*
n^+	normal coordinate (eq. (22))
P^+	pressure-gradient parameter (eq. (25))
p	pressure, $p^* \Big/ \left[\rho_\infty^* \left(U_\infty^*\right)^2\right]$
q^*	wall heat-transfer rate
r	radius measured from axis of symmetry to point on body surface, r^* / r_n^*
r_n^*	nose radius
s	coordinate measured along body surface, s^* / r_n^*
s_o	s at beginning of transition
$\bar{s}$	transition damping factor (eq. (35))
T	temperature, T^* / T_{ref}^*
T_{ref}^*	temperature, $\left(U_\infty^*\right)^2 / c_{p,\infty}^*$
U_∞^*	free-stream velocity
u	velocity component tangent to body surface, u^* / U_∞^*
u_τ	friction velocity (eq. (27))
v	velocity component normal to body surface, v^* / U_∞^*
v^+	scaled mean velocity component (eq. (26)), v_w / u_τ
$\bar{x}$	transition length scale

α shock angle defined in figure 1

$\left.\begin{matrix}\alpha_1,\alpha_2,\\ \alpha_3,\alpha_4\end{matrix}\right\}$ coefficients in equation (A8)

β angle defined in figure 1

γ ratio of specific heats

$\gamma_{i,\eta}$ normal intermittency factor (eq. (30))

$\gamma_{i,\xi}$ streamwise transition intermittency factor (eq. (34))

δ boundary-layer thickness

δ_k *incompressible displacement thickness* (eq. (29))

ϵ^+ normalized eddy viscosity (eq. (4)), μ_T/μ

ϵ_i^+ eddy viscosity, inner law (eq. (20))

ϵ_o^+ eddy viscosity, outer law (eq. (28))

η transformed n-coordinate, n/n_s

θ body angle defined in figure 1

κ body curvature

μ molecular viscosity, $\mu^*/\mu^*\left(T^*_{ref}\right)$

μ_T eddy viscosity (eq. (1))

ξ coordinate measured along body surface, $\xi = s$

ρ density of mixture, ρ^*/ρ^*_∞

σ Reynolds number parameter, $\left[\dfrac{\mu^*\left(T^*_{ref}\right)}{\rho^*_\infty U^*_\infty r^*_n}\right]^{1/2}$

ϕ quantity defined by equation (11a)

χ vorticity Reynolds number (eq. (33))

χ_c vorticity Reynolds number at beginning of transition

ψ quantity defined by equation (A10e)

Superscripts:

j 0 for plane flow; 1 for axisymmetric flow

$\overline{\quad}$ time-averaged quantity

* dimensional quantity

' total differential or fluctuating component

'' shock-oriented velocity component (see fig. 1)

Subscripts:

e boundary-layer edge

s shock

w wall

∞ free stream

Abbreviations:

BL boundary layer

VSL viscous shock layer

ANALYSIS

Governing Equations

The equations of motion for turbulent viscous shock layers are derived by methods analogous to those presented by Dorrance (ref. 6) for the turbulent-boundary-layer equations. The resulting equations for the shock-body coordinate system shown in figure 1 are presented in nondimensional form. For turbulent flow, time-averaged quantities are implied by the nomenclature, and the laminar-flow equations are obtained by neglecting the turbulent eddy viscosity and eddy thermal conductivity.

The eddy viscosity is expressed in time-averaged fluctuating components as

$$\mu_T = -\frac{\overline{(\rho v)' u'}}{\sigma^2 \frac{\partial u}{\partial n}} \tag{1}$$

and the eddy thermal conductivity is

$$k_T = -\frac{\overline{(\rho v)' h'}}{\sigma^2 \frac{\partial h}{\partial n}} \tag{2}$$

From the definition of the static turbulent Prandtl number

$$N_{Pr,T} = \frac{c_p \mu_T}{k_T} \tag{3}$$

and the definition

$$\epsilon^+ = \frac{\mu_T}{\mu} \tag{4}$$

the governing equations for the flow in laminar or turbulent viscous shock layers can be expressed as

Continuity:

$$\frac{\partial}{\partial s}\left[(r + n \cos \theta)^j \rho u\right] + \frac{\partial}{\partial n}\left[(1 + n\kappa)(r + n \cos \theta)^j \rho v\right] = 0 \tag{5}$$

s-momentum:

$$\rho\left(\frac{u}{1+n\kappa}\frac{\partial u}{\partial s}+v\frac{\partial u}{\partial n}+\frac{uv\kappa}{1+n\kappa}\right)+\frac{1}{1+n\kappa}\frac{\partial p}{\partial s}=\sigma^2\left\{\frac{\partial}{\partial n}\left[\mu(1+\epsilon^+)\frac{\partial u}{\partial n}-\frac{\mu u\kappa}{1+n\kappa}\right]\right.$$

$$\left.+\left(\frac{2\kappa}{1+n\kappa}+\frac{j\cos\theta}{r+n\cos\theta}\right)\left[\mu(1+\epsilon^+)\frac{\partial u}{\partial n}-\frac{\mu u\kappa}{1+n\kappa}\right]\right\} \tag{6}$$

n-momentum:

$$\rho\left(\frac{u}{1+n\kappa}\frac{\partial v}{\partial s}+v\frac{\partial v}{\partial n}-\frac{u^2\kappa}{1+n\kappa}\right)+\frac{\partial p}{\partial n}=0 \tag{7}$$

Energy:

$$\rho\left(\frac{u}{1+n\kappa}\frac{\partial H}{\partial s}+v\frac{\partial H}{\partial n}\right)-v\frac{\partial p}{\partial n}+\frac{\rho u^2 v\kappa}{1+n\kappa}=\sigma^2\left\{\frac{\partial}{\partial n}\left[\frac{\mu}{N_{Pr}}\left(1+\epsilon^+\frac{N_{Pr}}{N_{Pr,T}}\right)\frac{\partial H}{\partial n}+\phi\right]\right.$$

$$\left.+\left(\frac{\kappa}{1+n\kappa}+\frac{j\cos\theta}{r+n\cos\theta}\right)\left[\frac{\mu}{N_{Pr}}\left(1+\epsilon^+\frac{N_{Pr}}{N_{Pr,T}}\right)\frac{\partial H}{\partial n}+\phi\right]\right\} \tag{8}$$

State:

$$p=\frac{\gamma-1}{\gamma}\rho T \tag{9}$$

In these equations, the molecular viscosity as given by Sutherland's law is

$$\mu=\frac{1+C}{T+C}T^{3/2} \tag{10}$$

where

$$\phi=\frac{\mu}{N_{Pr}}\left[N_{Pr}-1+\frac{\epsilon^+ N_{Pr}}{N_{Pr,T}}\left(N_{Pr,T}-1\right)\right]u\frac{\partial u}{\partial n}-\frac{\mu u^2\kappa}{1+n\kappa} \tag{11a}$$

$$C = \frac{C^*}{(\gamma - 1)M_\infty^2 T_\infty^*} \tag{11b}$$

and

$$C^* = 110.33 \text{ K} \tag{11c}$$

The governing equations have a hyperbolic-parabolic nature (ref. 2), the hyperbolic nature arising from the normal-momentum equation. If the thin-shock-layer approximation is made, the normal-momentum equation becomes

$$\frac{\partial p}{\partial n} = \frac{\rho u^2 \kappa}{1 + n\kappa} \tag{12}$$

When equation (7) is replaced by equation (12), the resulting set of equations is parabolic. Consequently, the equations can be solved by using numerical methods similar to those used in solving boundary-layer problems. Equation (12) is used for an initial iteration; then for the final flow-field solution, equation (12) is replaced by equation (7), so that the thin-shock-layer approximation is removed.

Boundary Conditions

Conditions at the body surface.- The no-slip boundary conditions are used in this study. The surface conditions for $\eta = 0$ are

$$u = v = 0 \tag{13}$$

and for this study the temperature and enthalpy at the wall are specified as

$$T_W = H_W = \text{Constant} \tag{14}$$

Conditions at the shock.- The conditions imposed at the shock are calculated by using the Rankine-Hugoniot relations. The nondimensional shock relations are as follows:

Mass:

$$\rho_s v_s'' = -\sin \alpha \tag{15}$$

$$u_s'' = \cos \alpha \tag{16}$$

Momentum:

$$p_s = \frac{1}{\gamma_\infty M_\infty^2} + \sin^2 \alpha \left(1 - \frac{1}{\rho_s}\right) \tag{17}$$

Energy:

$$T_s = \frac{\left[2\gamma M_\infty^2 \sin^2 \alpha - (\gamma - 1)\right]\left[(\gamma - 1)M_\infty^2 \sin^2 \alpha + 2\right]}{(\gamma - 1)(\gamma + 1)^2 M_\infty^4 \sin^2 \alpha} \tag{18}$$

State:

$$\rho_s = \frac{\gamma p_s}{(\gamma - 1)T_s} \tag{19}$$

A transformation is applied to the previous nondimensional viscous-shock-layer equations and boundary conditions to simplify the numerical computations. The transformation relations and the transformed equations and boundary conditions are given in the appendix.

Eddy-Viscosity Approximations

A two-layer eddy-viscosity model consisting of an inner law based upon Prandtl's mixing-length concept and the Clauser-Klebanoff expression (based on refs. 7 and 8) for the outer law is used in the present investigation. This model, introduced by Cebeci (ref. 4), assumes that the inner law is applicable for the flow from the wall outward to the location where the eddy viscosity given by the inner law is equal to that of the outer law. The outer law is then assumed applicable for the remainder of the viscous layer. It is noted that the eddy viscosity degenerates to approximately zero in the inviscid portion of the shock layer. The degeneracy is expressed in terms of the normal intermittency factor given by Klebanoff (ref. 7). The expressions used in the present investigation are given in the following sections.

Inner-eddy-viscosity approximation.- Prandtl's mixing-length concept is stated in nondimensional variables as

$$\epsilon_i^+ = \frac{\rho \ell^2}{\sigma^2 \mu}\left|\frac{\partial u}{\partial n}\right| \tag{20}$$

The mixing length ℓ is evaluated by using Van Driest's proposal (ref. 9) stated as

$$\ell = k_1 n\left[1 - \exp\left(-\frac{n^+}{A^+}\right)\right] \tag{21}$$

where

$$n^+ = \frac{n\rho}{\sigma^2\mu}\left[\frac{\mu_w\left(\frac{\partial u}{\partial n}\right)_w}{\rho}\right]^{1/2} \tag{22}$$

Here, k_1 is the Von Kármán constant, which is assumed to have a value of 0.4, and A^+ is a damping factor.

Cebeci (ref. 4) suggests that for flows with a pressure gradient, the damping factor be expressed as

$$A^+ = 26(1 - 11.8P^+)^{-1/2} \tag{23}$$

and for flows with both a pressure gradient and mass injection,

$$A^+ = 26\left\{-\frac{P^+}{v^+}\left[\exp(11.8v^+) - 1\right] + \exp(11.8v^+)\right\}^{-1/2} \tag{24}$$

where

$$P^+ = -\sigma^2\left(\frac{\partial p}{\partial s}\right)_e \frac{\mu}{\rho^2 u_\tau^3} \tag{25}$$

$$v^+ = \frac{v_w}{u_\tau} \tag{26}$$

and

$$u_\tau = \sigma\left[\frac{\mu_w\left(\frac{\partial u}{\partial n}\right)_w}{\rho}\right]^{1/2} \tag{27}$$

Outer-eddy-viscosity approximation.- For the outer region of the viscous layer the eddy viscosity is approximated by the Clauser-Klebanoff expression

$$\epsilon_o^+ = \frac{k_2 \rho u_e \delta_k \gamma_{i,\eta}}{\sigma^2 \mu} \tag{28}$$

where

$$\delta_k = \int_0^\delta \left(1 - \frac{u}{u_e}\right) dn \tag{29}$$

$$k_2 = 0.0168$$

and

$$\gamma_{i,\eta} = \left[1 + 5.5\left(\frac{n}{\delta}\right)^6\right]^{-1} \tag{30}$$

Equation (30) is Cebeci's approximation (ref. 4) of the error-function definition presented by Klebanoff (ref. 7).

The boundary-layer thickness δ is assumed to be the value of n at the point where

$$\frac{H_t}{H_{t,\infty}} = 0.995 \tag{31}$$

and is determined by linear interpolation in an array of local total enthalpies. This definition is approximately equivalent to the usual boundary-layer definition

$$\frac{u}{u_e} = 0.995 \tag{32}$$

where u_e is the local value for the undisturbed inviscid flow outside the boundary layer.

The values of the parameters k_1 and k_2 in equations (21) and (28) depend on the flow conditions being considered, as does the constant represented by the value 26 in equations (23) and (24). The values given are used for convenience in developing the numerical method. For a discussion of these parameters, see reference 10.

Transition Models

Provisions for both continuous and instantaneous transition from laminar to turbulent flow have been included in the present investigation. Instantaneous transition is

initiated when the local Reynolds number or momentum-thickness Reynolds number exceeds a preselected value. Continuous transition is effected by defining a streamwise transition intermittency factor $\gamma_{i,\xi}$ which modifies the composite eddy viscosity ϵ^+ over an interval $\bar{x}$. The factor $\gamma_{i,\xi}$ is initially set to zero and is evaluated when the vorticity Reynolds number (proposed by Rouse, ref. 11, as the stability index)

$$\chi = \frac{n^2 \rho}{\sigma^2 \mu} \frac{\partial u}{\partial n} \tag{33}$$

exceeds a critical value χ_c. For the evaluation of $\gamma_{i,\xi}$, the relation

$$\gamma_{i,\xi} = 1 - \exp(-0.412\bar{s}) \tag{34}$$

was used, where

$$\bar{s} = \frac{4(s - s_o)}{s_o(\bar{x} - 1)} \tag{35}$$

This model was developed by Dhawan and Narasimha (ref. 12) on the basis of the experimental data presented by Owen (ref. 13). Approximate values of χ_c and $\bar{x}$ are

$$2000 \leqq \chi_c \leqq 4000$$

and

$$\bar{x} \approx 2$$

The values of χ_c and $\bar{x}$ are strongly influenced by the body shape and flow conditions being considered and are more appropriately defined by comparison with experimental data. A discussion of these parameters is given by Harris (ref. 10).

Method of Solution

The procedure for solving the viscous-shock-layer equations is presented herein. First, the finite-difference expressions used to transform the differential equations to algebraic equations are presented. Then the solution procedure is discussed.

Finite-difference expressions.- The derivatives are converted to finite-difference form by using Taylor's series expansions. A variable grid spacing (fig. 2) is used in the η-direction so that the grid spacing can be made small in the region of large gradients.

Three-point differences are used in the η-direction, and two-point, fully implicit differences are used in the ξ-direction. Truncation terms of order $\Delta\xi_m$ (first-order accuracy) and either $\Delta\eta_n\Delta\eta_{n-1}$ or $\Delta\eta - \Delta\eta_{n-1}$ (second-order accuracy) are neglected. A typical finite-difference expansion of the standard differential equation (see eq. (A8)) gives

$$A_n W_{m,n-1} + B_n W_{m,n} + C_n W_{m,n+1} = D_n \tag{36}$$

The coefficients A, B, C, and D are used to represent the coefficients after the finite-difference expansion of equation (A8). The subscript n denotes the grid points along a line normal to the body surface, whereas the subscript m denotes the grid stations along the body surface. Equation (36) along with the boundary conditions constitutes a system of the tridiagonal form, for which efficient computational procedures are available. (See ref. 14.)

Overall solution procedure.- For specified free-stream conditions and body geometry, a stagnation-streamline solution is obtained. With the stagnation-streamline solution providing the initial conditions, the conditions at the shock providing the outer boundary conditions, and the conditions at the wall taken as the inner boundary conditions, the numerical solution is marched downstream to the desired body location ξ. The first solution pass provides only an approximate flow-field solution, because the following assumptions are used in the first solution pass:

(a) The thin-shock-layer form of the n-momentum equation (eq. (A12b)) is used.

(b) The stagnation-streamline solution is independent of downstream influence (approximation of local similarity where $n_{2,s} = 0$).

(c) The term $dn_s/d\xi$ is equated to zero at each body station.

(d) The shock angle α is assumed to be the same as the body angle θ.

These assumptions are then removed by making one or more additional solution passes. For the current study, a total of two solution passes are used since the two passes resulted in a converged flow-field solution. For the second solution pass, the thin-shock-layer form of the normal-momentum equation (eq. (A12b)) is replaced by equation (A12a). The $\bar{v}$ component of velocity that is used in equation (A12a) is the value from the previous solution pass. Also, once the first solution pass has been computed, the values of $n_{2,s}$ and $dn_s/d\xi$ are calculated and used in the second solution pass to remove approximations (b), (c), and (d). Hence, the viscous-shock-layer equations are solved as parabolic equations, and yet retain effects which are elliptic and hyperbolic in nature. This solution procedure is programed for the Control Data Corporation 6600 computer. The execution time is approximately 0.03 second per grid point for a converged solution. (This includes all local iterations and solution passes.)

Shock solution.- The shock solution procedure at any location is identical for the first and subsequent solution passes. However, the shock angle α is defined differently for the first and subsequent solution passes and is set equal to the local body angle θ for the first solution pass. For subsequent solution passes, the shock angle is defined as

$$\alpha = \theta + \tan^{-1} \frac{n_s'}{1 + \kappa n_s} \tag{37}$$

Solution procedure at station m.- The viscous-shock-layer equations are solved at any body station m (see fig. 2) in the order shown in figure 3. The governing equations are uncoupled and the dependent variables are solved one at a time, also in the order shown in figure 3. First, the shock conditions are calculated to establish the outer boundary conditions. Then the converged profiles at station m - 1 are used as the initial guess for the profiles at station m. The solution is then iterated locally until convergence is achieved. For the stagnation streamline (m = 1), guess values for the profiles are used to start the solution.

The first-order equations are numerically integrated by means of the trapezoid rule. Each of the second-order partial differential equations is individually integrated numerically by using the tridiagonal formalism (eq. (36)). The global-continuity equation is used to obtain both the shock standoff distance and the $\bar{v}$ components of velocity. By integrating equation (A11) between the limits of $\eta = 0$ and $\eta = 1$ at station m, an implicit equation for n_s is obtained. For the $\bar{v}$ component of velocity at η, equation (A11) is integrated with respect to η between the limits of 0 to η. The pressure $\bar{p}$ is determined at station m by integrating the normal-momentum equations (A12) with respect to η between the limits of 1 to η. The equation of state is used to determine the density.

DISCUSSION AND RESULTS

Comparisons are made between the present viscous-shock-layer analysis and turbulent-boundary-layer solutions obtained with the computer program described in reference 15. For the data presented, fully developed turbulent flow without mass injection has been assumed. However, provisions have been included for the analysis of continuous or instantaneous transition and for mass injection at the surface.

Results are presented for a Mach 19 flow about a 45° (total angle) hyperboloid with a nose radius of 0.3048 meter for free-stream Reynolds numbers of 3.1×10^6 and 12.4×10^6. The wall temperature is taken to be one-tenth of the stagnation temperature, and the free-stream temperature is 256 K. The Prandtl number and the turbulent Prandtl number are assumed to be 0.72 and 0.90, respectively.

The combination of high Reynolds numbers and low-wall-temperature results in boundary-layer thicknesses which are less than 10 percent of the total shock-layer thickness and imposes severe resolution requirements upon the numerical method. The solutions presented have been obtained with 150 grid points across the shock layer, the ratio of adjacent step sizes being a constant value equal to 1.08 (geometric progression). This choice of the grid-point distribution results in approximately 80 points within the predominantly viscous portion of the shock layer. More recent calculations have shown that 100 grid points across the shock layer having the same constant step-size ratio provide adequate resolution. The differences in the solutions obtained with 150 and 100 grid points are less than ±1 percent. However, the use of 75 grid points across the shock layer results in solutions which differ by as much as 30 to 40 percent for the wall measurable quantities. For laminar flows with low Reynolds number and a higher ratio of wall temperature to stagnation temperature, as few as 50 grid points can be used.

Distributions of boundary-layer thickness, incompressible displacement thickness, heat transfer, and skin friction calculated by the present analysis and by boundary-layer theory are shown in figures 4, 5, 6, and 7, respectively. Inspection of these results shows that maximum differences between the two methods are less than ±10 percent for all parameters. The heat-transfer distribution corresponding to a Newtonian surface pressure distribution as input to the boundary-layer computer program is shown in figure 6 for a free-stream Reynolds number of 3.1×10^6. Less severe conditions than those for the cases presented result in essentially identical solutions from the two methods of analysis.

Representative comparisons of the eddy-viscosity profiles for a free-stream Reynolds number of 3.1×10^6 are shown for body stations s^*/r_n^* of 0.5 and 3.5 in figure 8. At the downstream location, maximum differences in the eddy viscosities are less than ±10 percent. For the body station in the nose region, differences as large as 30 percent are noted for n^*/r_n^* near the boundary-layer edge. These differences were found to have little influence upon the solution. Transition criteria indicate that the flow at the station in the nose region is laminar.

Figures 9 and 10 show velocity profiles calculated by the viscous-shock-layer and boundary-layer solution methods for $N_{Re} = 3.1 \times 10^6$ at $s^*/r_n^* = 2$ and $s^*/r_n^* = 80$, respectively. The data shown in figure 9 for $s^*/r_n^* = 2$ correspond to a location where the effects of streamline swallowing are negligible. For this body station, the profiles corresponding to boundary-layer and viscous-shock-layer solutions differ by less than ±5 percent for $n^*/r_n^* \leq 0.8\delta$. At the downstream body station $s^*/r_n^* = 80$ (fig. 10), the agreement between the profiles calculated by the two methods is poor, since the boundary-layer analysis does not account for the effect of streamline swallowing. The edge conditions for the boundary-layer solution correspond to an isentropic expansion of the gas from the stagnation point of the body. For the viscous-shock-layer solution, the edge

conditions correspond to the flow which crosses the weaker portions of the bow shock, where the entropy jump across the shock is much less than at the stagnation streamline. For the 45° (total angle) hyperboloid considered, the asymptotic limit approaches the solution for an equivalent cone. For the body station $s^*/r_n^* = 80$, the conditions at the edge of the boundary layer as calculated with the viscous-shock-layer analysis differ from the cone solution by less than 1 percent. The surface pressure corresponding to the viscous-shock-layer solution at this station is approximately 15 percent higher than the corresponding inviscid cone solution. However, as previously mentioned, in the outer inviscid region the solution is approximately the same as the asymptotic cone solution. The increase in pressure through the predominantly viscous layer was also noted by Mayne and Adams (ref. 1) for laminar flow. For laminar flows, the viscous-shock-layer solution used in the present analysis is the same as that used in reference 1. Results for laminar flows are not presented.

Heat-transfer distributions corresponding to the viscous-shock-layer and boundary-layer solutions for $N_{Re} = 3.1 \times 10^6$ are shown in figure 11. The two solutions show the expected differences, and the viscous-shock-layer analysis appears to account correctly for streamline swallowing. However, the boundary-layer analysis used in the present study does not account for streamline swallowing, and the accuracy of the viscous-shock-layer analysis must be assessed by comparison with an appropriately modified boundary-layer analysis.

For the solution of the turbulent-viscous-shock-layer equations, the use of Klebanoff's intermittency factor (ref. 7) is essential, whereas in boundary-layer solutions, the intermittency factor may be assumed unity without significantly influencing the results obtained. (See ref. 16.) For the viscous-shock-layer equations, the use of a unit intermittency factor results in an increase in heat transfer and skin friction of 30 to 50 percent for $s^*/r_n^* > 2$. This difference in behavior of the viscous-shock-layer and boundary-layer solutions is the result of the nonvanishing tangential velocity gradients in the normal-coordinate direction. (See fig. 9.) For the boundary-layer equations, the boundary conditions imposed ensure that the gradients in the normal-coordinate direction approach zero at the boundary-layer edge.

CONCLUSIONS

Equations describing the turbulent viscous shock layers over blunt axially symmetric bodies of analytic shape are presented for hypersonic flow of a perfect gas. A two-layer eddy-viscosity model consisting of an inner law based upon Prandtl's mixing-length concept and the Clauser-Klebanoff expression for the outer law is used in the present study. Methods for defining the boundary-layer thickness and incompressible boundary-layer displacement thickness which are consistent with boundary-layer theory are pre-

sented. An implicit finite-difference technique for solving the equations is given. Comparisons of the present results with previously reported boundary-layer solutions are made for a Mach 19 flow over a 45^{o} hyperboloid. The free-stream Reynolds numbers are 3.1×10^{6} and 12.4×10^{6}, whereas the wall temperature is one-tenth of the stagnation temperature.

Results of the study lead to the following conclusions:

1. The present results are in good agreement with classical boundary-layer results in regions where the effects of streamline swallowing are negligible. However, for the downstream locations, where streamline swallowing effects are present, expected differences between the present results and the classical boundary-layer results are evident.

2. For the solution of the turbulent-viscous-shock-layer equations, the use of Klebanoff's normal intermittency factor is essential. This is in marked contrast with turbulent-boundary-layer solutions, where the normal intermittency factor may be assumed unity without significantly influencing the results.

3. For the flow conditions considered, a boundary-layer thickness (required in the eddy-viscosity model) based on a total-enthalpy ratio provides good agreement with boundary-layer results.

Langley Research Center,
National Aeronautics and Space Administration,
Hampton, Va., January 21, 1975.

APPENDIX

TRANSFORMED VISCOUS-SHOCK-LAYER EQUATIONS

This appendix presents the transformed viscous-shock-layer equations and boundary conditions. First, the relations defining the transformed variables and coordinates are given. Next, the general equations and boundary conditions are given. Then, the special form of the equations for the stagnation streamline are developed along with the stagnation shock relations.

Transformation Relations

To simplify the numerical computations, a transformation is applied to the viscous-shock-layer equations. This transformation is accomplished by normalizing most of the variables by their local shock values. When the normal coordinate is normalized with respect to the local shock standoff distance, a constant number of finite-difference grid points between the body and shock are used. This procedure eliminates the need for interpolation to determine shock shape and the addition of grid points in the normal direction as the computation moves downstream.

The transformed variables are

$$\left.\begin{array}{lll} \eta = \dfrac{n}{n_s} & \bar{p} = \dfrac{p}{p_s} & \bar{\mu} = \dfrac{\mu}{\mu_s} \\ \xi = s & \bar{\rho} = \dfrac{\rho}{\rho_s} & \bar{a}_0 = \dfrac{a_0}{a_{0,s}} \\ \bar{u} = \dfrac{u}{u_s} & \bar{T} = \dfrac{T}{T_s} & \bar{a}_1 = \dfrac{a_1}{a_{1,s}} \\ \bar{v} = \dfrac{v}{v_s} & \bar{H} = \dfrac{H}{H_s} & \bar{a}_2 = \dfrac{a_2}{a_{2,s}} \end{array}\right\} \tag{A1}$$

where bars over the quantities denote normalization with respect to the shock value. The transformations relating the differential quantities are

$$\frac{\partial}{\partial s} = \frac{\partial}{\partial \xi} - \frac{n_s'}{n_s}\eta\frac{\partial}{\partial \eta} \tag{A2}$$

where

$$n_s' = \frac{dn_s}{d\xi} \tag{A3}$$

$$\frac{\partial}{\partial n} = \frac{1}{n_s}\frac{\partial}{\partial \eta} \tag{A4}$$

and

$$\frac{\partial^2}{\partial n^2} = \frac{1}{{n_s}^2}\frac{\partial^2}{\partial \eta^2} \tag{A5}$$

The transformations used to express the shock-oriented velocities u_s'' and v_s'' in terms of the body-oriented coordinate system (fig. 1) are

$$u_s = u_s'' \sin(\alpha + \beta) + v_s'' \cos(\alpha + \beta) \tag{A6}$$

and

$$v_s = -u_s'' \cos(\alpha + \beta) + v_s'' \sin(\alpha + \beta) \tag{A7}$$

Transformed Equations

After the governing equations are written in transformed variables and coordinates, the second-order partial differential equations are written in the following form:

$$\frac{\partial^2 W}{\partial \eta^2} + \alpha_1 \frac{\partial W}{\partial \eta} + \alpha_2 W + \alpha_3 + \alpha_4 \frac{\partial W}{\partial \xi} = 0 \tag{A8}$$

The quantity W represents $\bar{u}$ in the s-momentum equation and $\overline{H}$ in the energy equation. The coefficients α_1 to α_4 are written as follows:

s-momentum, $W = \bar{u}$:

$$\alpha_1 = \frac{1}{\bar{a}_0}\frac{\partial \bar{a}_0}{\partial \eta} + \frac{n_s \kappa}{1 + n_s \eta \kappa}\left(2 - \frac{\mu_s \bar{\mu}}{a_{0,s}\bar{a}_0}\right) + \frac{j n_s \cos\theta}{r + n_s \eta \cos\theta} + \frac{n_s \rho_s u_s n_s'}{\sigma^2 a_{0,s}(1 + n_s \eta \kappa)}\frac{\bar{\rho}\bar{u}\bar{\eta}}{\bar{a}_0} - \frac{n_s \rho_s v_s}{\sigma^2 a_{0,s}}\frac{\bar{\rho}\bar{v}}{\bar{a}_0} \tag{A9a}$$

$$\alpha_2 = -\frac{\kappa n_s}{1 + n_s\eta\kappa}\frac{1}{\bar{a}_0}\frac{\partial\bar{a}_0}{\partial\eta} - \frac{n_s^2\kappa}{1 + n_s\eta\kappa}\left(\frac{\kappa}{1 + n_s\eta\kappa} + \frac{j\cos\theta}{r + n_s\eta\cos\theta}\right)\frac{\mu_s\bar{\mu}}{a_{0,s}\bar{a}_0}$$

$$- \frac{\rho_s n_s^2 u_s'}{\sigma^2 a_{0,s}(1 + n_s\eta\kappa)}\frac{\bar{u}\bar{\rho}}{\bar{a}_0} - \frac{n_s^2\rho_s v_s\kappa}{\sigma^2 a_{0,s}(1 + n_s\eta\kappa)}\frac{\bar{\rho}\bar{v}}{\bar{a}_0} \tag{A9b}$$

$$\alpha_3 = -\frac{p_s n_s^2}{\sigma^2 a_{0,s} u_s(1 + n_s\eta\kappa)\bar{a}_0}\left(\frac{\partial\bar{p}}{\partial\xi} + \frac{p_s'\bar{p}}{p_s} - \frac{n_s'\eta}{n_s}\frac{\partial\bar{p}}{\partial\eta}\right) \tag{A9c}$$

$$\alpha_4 = -\frac{\rho_s u_s n_s^2}{\sigma^2 a_{0,s}(1 + n_s\eta\kappa)}\frac{\bar{\rho}\bar{u}}{\bar{a}_0} \tag{A9d}$$

where

$$a_0 = \mu(1 + \epsilon^+) \tag{A9e}$$

Energy, $W = \bar{\bar{H}}$:

$$\alpha_1 = \frac{1}{\bar{a}_1}\frac{\partial\bar{a}_1}{\partial\eta} + n_s\left(\frac{\kappa}{1 + n_s\eta\kappa} + \frac{j\cos\theta}{r + n_s\eta\cos\theta}\right) + \frac{\rho_s n_s}{\sigma^2 a_{1,s}\bar{a}_1}\left(\frac{n_s' u_s\eta\bar{u}\bar{\rho}}{1 + n_s\eta\kappa} - v_s\bar{\rho}\bar{v}\right) \tag{A10a}$$

$$\alpha_2 = \frac{\alpha_4 H_s'}{H_s} \tag{A10b}$$

$$\alpha_3 = \frac{n_s^2}{a_{1,s}\bar{a}_1 H_s}\left[\frac{1}{n_s}\frac{\partial\psi}{\partial\eta} + \left(\frac{\kappa}{1 + n_s\eta\kappa} + \frac{j\cos\theta}{r + n_s\eta\cos\theta}\right)\psi\right] \tag{A10c}$$

$$\alpha_4 = -\frac{n_s^2\rho_s u_s\bar{u}\bar{\rho}}{\sigma^2 a_{1,s}(1 + n_s\eta\kappa)\bar{a}_1} \tag{A10d}$$

where

$$\psi = u_s{}^2\bar{u}\left(\frac{a_{2,s}\bar{a}_2}{n_s}\frac{\partial\bar{u}}{\partial\eta} - \frac{\kappa\mu_s}{1+\eta n_s\kappa}\bar{\mu}\bar{u}\right) \tag{A10e}$$

$$a_1 = \frac{\mu}{N_{Pr}}\left(1 + \frac{\epsilon^+ N_{Pr}}{N_{Pr,T}}\right) \tag{A10f}$$

$$a_2 = \frac{\mu}{N_{Pr}}\left[N_{Pr} - 1 + \frac{\epsilon^+ N_{Pr}}{N_{Pr,T}}\left(N_{Pr,T} - 1\right)\right] \tag{A10g}$$

The preceding energy equation is for the thin-shock-layer approximation. When equation (7) is used for the n-momentum equation, the following term must be added to equation (A10c):

$$\frac{n_s v_s \bar{v}}{\sigma^2 a_{1,s} H_s \bar{a}_1}\left(p_s\frac{\partial\bar{p}}{\partial\eta} - \frac{n_s u_s{}^2 \rho_s \kappa}{1+\eta n_s\kappa}\bar{\rho}\bar{u}^2\right) \tag{A10h}$$

The remaining equations are written as follows:

Global continuity:

$$\frac{\partial}{\partial\xi}\left[n_s(r + n_s\eta\cos\theta)^j\rho_s u_s\bar{\rho}\bar{u}\right] + \frac{\partial}{\partial\eta}\left\{(r + n_s\eta\cos\theta)^j\left[(1 + n_s\eta\kappa)\rho_s v_s\bar{\rho}\bar{v} - n_s'\eta\rho_s u_s\bar{\rho}\bar{u}\right]\right\} = 0 \tag{A11}$$

n-momentum:

$$\frac{\bar{\rho}\bar{u}}{1+n_s\eta\kappa}\left(\frac{v_s'}{v_s}\bar{v} + \frac{\partial\bar{v}}{\partial\xi} - \frac{n_s'\eta}{n_s}\frac{\partial\bar{v}}{\partial\eta}\right) + \frac{v_s}{u_s}\frac{\bar{\rho}\bar{v}}{n_s}\frac{\partial\bar{v}}{\partial\eta} - \frac{u_s}{v_s}\frac{\kappa}{1+n_s\eta\kappa}\bar{\rho}\bar{u}^2 + \frac{p_s}{\rho_s u_s n_s v_s}\frac{\partial\bar{p}}{\partial\eta} = 0 \tag{A12a}$$

which, if the thin-shock-layer approximation is made, becomes

$$\frac{\partial \bar{p}}{\partial \eta} = \frac{n_s \rho_s u_s^2 \kappa}{p_s(1 + n_s \eta \kappa)} \bar{\rho} \bar{u}^2 \tag{A12b}$$

State:

$$\bar{p} = \bar{\rho} \overline{T} \tag{A13}$$

Equations (A8) to (A13) along with the appropriate boundary conditions are the governing relations used to describe the viscous shock layer for a perfect gas.

Boundary Conditions

Conditions at the body surface.- The surface boundary conditions in terms of transformed variables are

$$\bar{u} = \bar{v} = 0 \tag{A14}$$

$$\overline{T}_w = \overline{H}_w = \text{Constant} \tag{A15}$$

Conditions at the shock.- The shock conditions are determined by solving equations (15) to (19). The transformed shock conditions become

$$\bar{u} = \overline{T} = \overline{H} = \bar{v} = \bar{\rho} = \bar{p} = \bar{\mu} = \bar{a}_0 = \bar{a}_1 = \bar{a}_2 = 1 \tag{A16}$$

at $\eta = 1$.

Stagnation-Streamline Equations

When downstream numerical solutions are required, it is necessary to have an accurate solution for the flow along the stagnation streamline. A truncated series, which has the same form as that used by Kao in reference 17, is used to develop the stagnation-streamline equations. The flow is assumed to be laminar along the stagnation streamline. The flow variables are expanded about the axis of symmetry with respect to the nondimensional distance ξ along the body as follows:

$$p(\xi,\eta) = p_1(\eta) + p_2(\eta)\xi^2 + \ldots \tag{A17a}$$

$$u(\xi,\eta) = u_1(\eta)\xi + \ldots \tag{A17b}$$

$$v(\xi,\eta) = v_1(\eta) + \ldots \tag{A17c}$$

$$\rho(\xi,\eta) = \rho_1(\eta) + \ldots \tag{A17d}$$

$$T(\xi,\eta) = T_1(\eta) + \ldots \tag{A17e}$$

$$h(\xi,\eta) = h_1(\eta) + \ldots \tag{A17f}$$

$$\mu(\xi,\eta) = \mu_1(\eta) + \ldots \tag{A17g}$$

The shock standoff distance is written as

$$n_s = n_{1,s} + n_{2,s}\xi^2 + \ldots \tag{A18}$$

Furthermore, ξ is small and the curvature κ is approximately 1 in the stagnation region. Consequently, the geometric relations (see fig. 1), including terms of order ξ, can be written as

$$\beta \approx \xi \tag{A19}$$

and

$$\alpha \approx \frac{\pi}{2} + \xi\left(\frac{2n_{2,s}}{1 + n_{1,s}} - 1\right) \tag{A20}$$

Therefore,

$$\sin(\alpha + \beta) \approx 1 \tag{A21}$$

and

$$\cos(\alpha + \beta) \approx \frac{2n_{2,s}\xi}{1 + n_{1,s}} \tag{A22}$$

The shock relations (eqs. (15) to (19)) in terms of expanded variables become

$$v_s = v_{1,s} + \ldots \approx -\frac{1}{\rho_{1,s}} = -\frac{M_\infty{}^2(\gamma - 1) + 2}{M_\infty{}^2(\gamma + 1)} \tag{A23}$$

$$u_s = u_{1,s}\xi + \ldots \approx \xi\left[1 - \frac{2n_{2,s}}{1 + n_{1,s}}\left(1 - \frac{1}{\rho_{1,s}}\right)\right] \tag{A24}$$

$$p_s = p_{1,s} + p_{2,s}\xi^2 + \ldots \approx \frac{1}{\gamma M_\infty{}^2} + \left(1 - \frac{1}{\rho_{1,s}}\right) - \xi^2\left[\left(1 - \frac{1}{\rho_{1,s}}\right)\left(1 - \frac{2n_{2,s}}{1 + n_{1,s}}\right)^2\right] \tag{A25}$$

and

$$T_s = T_{1,s} + \ldots \approx \frac{1}{M_\infty{}^2\left(\gamma_\infty - 1\right)} + \frac{1}{2}\left(1 - \frac{1}{\rho_{1,s}}\right) \tag{A26}$$

An examination of these equations shows that the equations for u_s and p_s contain $n_{2,s}$. This term cannot be determined from the stagnation solutions, since it is a function of the downstream flow. Consequently, a value must be assumed for $n_{2,s}$. In this study, it is assumed to be zero to start the solution, but this assumption is then removed by iterating on the solution with the previous shock standoff distances used to define $n_{2,s}$. The effect of the downstream shock shape on the stagnation-point solution is elliptic rather than parabolic.

Along the stagnation streamline, the second-order differential equations are written as

$$\frac{d^2W}{d\eta^2} + \alpha_1\frac{dW}{d\eta} + \alpha_2 W + \alpha_3 = 0 \tag{A27}$$

The coefficients are defined as

s-momentum, $W = \bar{u}$:

$$\alpha_1 = \frac{1}{\bar{\mu}_1}\frac{d\bar{\mu}_1}{d\eta} + (j + 1)\frac{n_{1,s}}{1 + n_{1,s}\eta} - \frac{n_{1,s}\rho_{1,s}v_{1,s}}{\sigma^2\mu_{1,s}}\frac{\bar{\rho}_1\bar{v}_1}{\bar{\mu}_1} \tag{A28a}$$

$$\alpha_2 = -\frac{n_{1,s}}{1 + n_{1,s}\eta}\left[\frac{1}{\bar{\mu}_1}\frac{d\bar{\mu}_1}{d\eta} + \frac{n_{1,s}}{1 + n_{1,s}\eta}(j + 1) + \frac{\rho_{1,s}n_{1,s}u_{1,s}}{\sigma^2\mu_{1,s}}\frac{\bar{\rho}_1\bar{u}_1}{\bar{\mu}_1} + \frac{n_{1,s}\rho_{1,s}v_{1,s}}{\sigma^2\mu_{1,s}}\frac{\bar{\rho}_1\bar{v}_1}{\bar{\mu}_1}\right] \tag{A28b}$$

$$\alpha_3 = \frac{-2p_{1,s}n_{1,s}^2}{\sigma^2\mu_{1,s}\left(1 + n_{1,s}\eta\right)u_{1,s}\bar{\mu}}\left(\bar{p}_2 + \frac{p_{2,s}\bar{p}_1}{p_{1,s}} - \frac{n_{2,s}\eta}{n_{1,s}}\frac{d\bar{p}_1}{d\eta}\right) \tag{A28c}$$

Energy (enthalpy), $W = \overline{H}$:

$$\alpha_1 = \frac{1}{\bar{\mu}_1}\frac{d\bar{\mu}_1}{d\eta} - \frac{1}{N_{Pr,1}}\frac{d\overline{N}_{Pr,1}}{d\eta} + \frac{(j + 1)n_{1,s}}{1 + n_{1,s}\eta} - \frac{n_{1,s}\rho_{1,s}\left(N_{Pr,1}\right)_s v_{1,s}}{\sigma^2\mu_{1,s}}\frac{\bar{\rho}_1\overline{N}_{Pr,1}\bar{v}_1}{\bar{\mu}_1} \tag{A29a}$$

$$\alpha_2 = 0 \tag{A29b}$$

$$\alpha_3 = 0 \tag{A29c}$$

The preceding energy equation is for the thin-shock-layer approximation. When equation (7) is used for the n-momentum equation, the following term must be added to equation (A29c):

$$\frac{n_{1,s}v_{1,s}p_{1,s}\left(N_{Pr,1}\right)_s}{\sigma^2\mu_{1,s}H_{1,s}}\frac{N_{Pr,1}\bar{v}_1}{\bar{\mu}_1}\frac{d\bar{p}}{d\eta}$$

The remaining equations are written as follows:

Global continuity:

$$\frac{d}{d\eta}\left[\left(1 + n_{1,s}\eta\right)^{j+1}\rho_{1,s}v_{1,s}\bar{\rho}_1\bar{v}_1\right] = -(j + 1)n_{1,s}\left(1 + n_{1,s}\eta\right)^j\rho_{1,s}u_{1,s}\bar{\rho}_1\bar{u}_1 \tag{A30}$$

n-momentum:

$$\frac{d\bar{p}_1}{d\eta} = -\frac{v_{1,s}^2 \rho_{1,s}}{\bar{p}_{1,s}} \bar{\rho}_1 \bar{v}_1 \frac{d\bar{v}_1}{d\eta} \tag{A31a}$$

When the thin-shock-layer approximation is made, the n-momentum equation becomes

$$\frac{d\bar{p}_1}{d\eta} = 0 \tag{A31b}$$

The $\bar{p}_2$ term that appears in equation (A28c) can be expressed as

$$\frac{d\bar{p}_2}{d\eta} = \frac{\rho_{1,s} u_{1,s}^2 n_{1,s}}{p_{1,s}} \frac{\bar{\rho}_1 \bar{u}_1^2}{1 + \eta n_{1,s}} + \frac{2\rho_{1,s} u_{1,s} n_{2,s} v_{1,s}}{p_{1,s}} \frac{\bar{\rho}_1 \bar{u}_1 \eta}{1 + \eta n_{1,s}} \frac{d\bar{v}_1}{d\eta} + \frac{p_{2,s} \rho_{1,s} v_{1,s}^2}{p_{1,s}^2} \bar{\rho}_1 \bar{v}_1 \frac{d\bar{v}_1}{d\eta} \tag{A31c}$$

For the thin-shock-layer approximation, this term is

$$\frac{d\bar{p}_2}{d\eta} = \frac{\rho_{1,s} u_{1,s}^2 n_{1,s}}{p_{1,s}} \frac{\bar{\rho}_1 \bar{u}_1^2}{1 + \eta n_{1,s}} \tag{A31d}$$

These equations along with the equation of state constitute the nonlinear ordinary differential equations that are solved along the stagnation streamline.

REFERENCES

1. Mayne, A. W., Jr.; and Adams, J. C., Jr.: Streamline Swallowing by Laminar Boundary Layers in Hypersonic Flow. AEDC-TR-71-32, U.S. Air Force, Mar. 1971. (Available from DDC as AD 719 749.)

2. Davis, R. T.: Numerical Solution of the Hypersonic Viscous Shock-Layer Equations. AIAA J., vol. 8, no. 5, May 1970, pp. 843-851.

3. Eaton, R. R.; and Larson, D. E.: Laminar and Turbulent Viscous Shock Layer Flow in the Symmetry Planes of Bodies at Angle of Attack. AIAA Paper No. 74-599, June 1974.

4. Cebeci, Tuncer: Behavior of Turbulent Flow Near a Porous Wall With Pressure Gradient. AIAA J., vol. 8, no. 12, Dec. 1970, pp. 2152-2156.

5. Anderson, E. C.; and Lewis, C. H.: Laminar or Turbulent Boundary-Layer Flows of Perfect Gases or Reacting Gas Mixtures in Chemical Equilibrium. NASA CR-1893, 1971.

6. Dorrance, William H.: Viscous Hypersonic Flow. McGraw-Hill Book Co., Inc., c.1962.

7. Klebanoff, P. S.: Characteristics of Turbulence in a Boundary Layer With Zero Pressure Gradient. NACA Rep. 1247, 1955. (Supersedes NACA TN 3178.)

8. Clauser, Francis H.: The Turbulent Boundary Layer. Vol. IV of Advances in Applied Mechanics, H. L. Dryden and Th. von Kármán, eds., Academic Press, Inc., 1956, pp. 1-51.

9. Van Driest, E. R.: On Turbulent Flow Near a Wall. J. Aeronaut. Sci., vol. 23, no. 11, Nov. 1956, pp. 1007-1011, 1036.

10. Harris, Julius E.: Numerical Solutions of the Equations for Compressible Laminar, Transitional, and Turbulent Boundary Layers and Comparisons With Experimental Data. NASA TR R-368, 1971.

11. Rouse, Hunter: A General Stability Index for Flow Near Plane Boundaries. J. Aeronaut. Sci., vol. 12, no. 4, Oct. 1945, pp. 423-431.

12. Dhawan, S.; and Narasimha, R.: Some Properties of Boundary Layer Flow During the Transition From Laminar to Turbulent Motion. J. Fluid Mech., vol. 3, pt. 4, Jan. 1958, pp. 418-436.

13. Owen, F. K.: Transition Experiments on a Flat Plate at Subsonic and Supersonic Speeds. AIAA J., vol. 8, no. 3, Mar. 1970, pp. 518-523.

14. Conte, S. D.: Elementary Numerical Analysis. McGraw-Hill Book Co., Inc., c.1965.

15. Miner, E. W.; Anderson, E. C.; and Lewis, Clark H.: A Computer Program for Two-Dimensional and Axisymmetric Nonreacting Perfect Gas and Equilibrium Chemically Reacting Laminar, Transitional, and/or Turbulent Boundary Layer Flows. VPI-E-71-8, May 1971. (Available as NASA CR-132601.)

16. Lewis, Clark H.; Miner, E. W.; and Anderson, E. C.: Effects of Strong Axial Pressure Gradients on Turbulent Boundary-Layer Flows. Turbulent Shear Flows, AGARD-CP-93, Jan. 1972, pp. 21-1 – 21-14.

17. Kao, Hsiao C.: Hypersonic Viscous Flow Near the Stagnation Streamline of a Blunt Body: I. A Test of Local Similarity. AIAA J., vol. 2, no. 11, Nov. 1964, pp. 1892-1897.

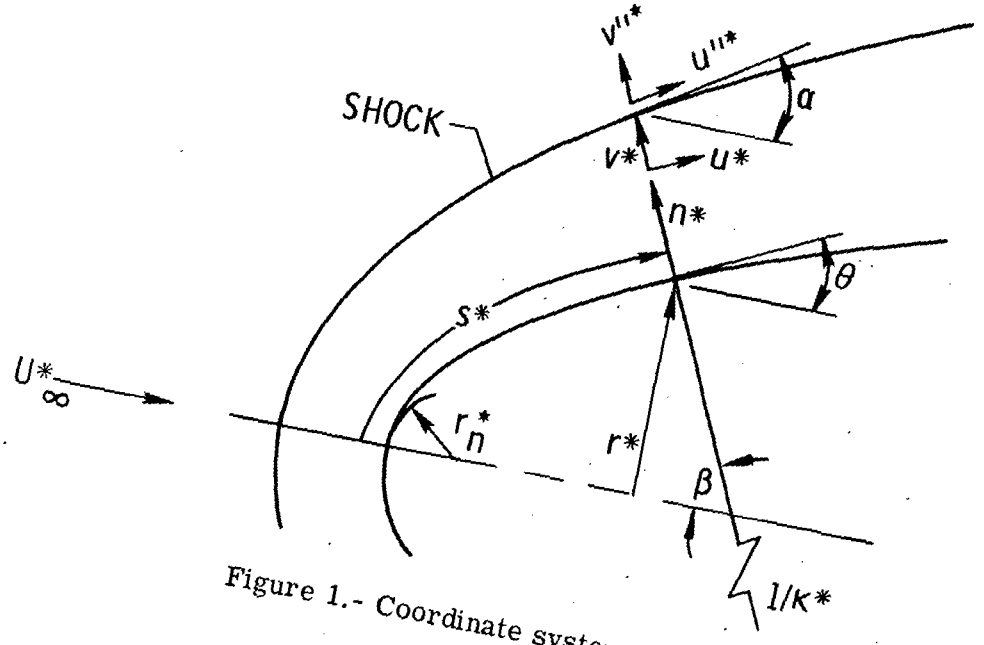

Figure 1.- Coordinate system.

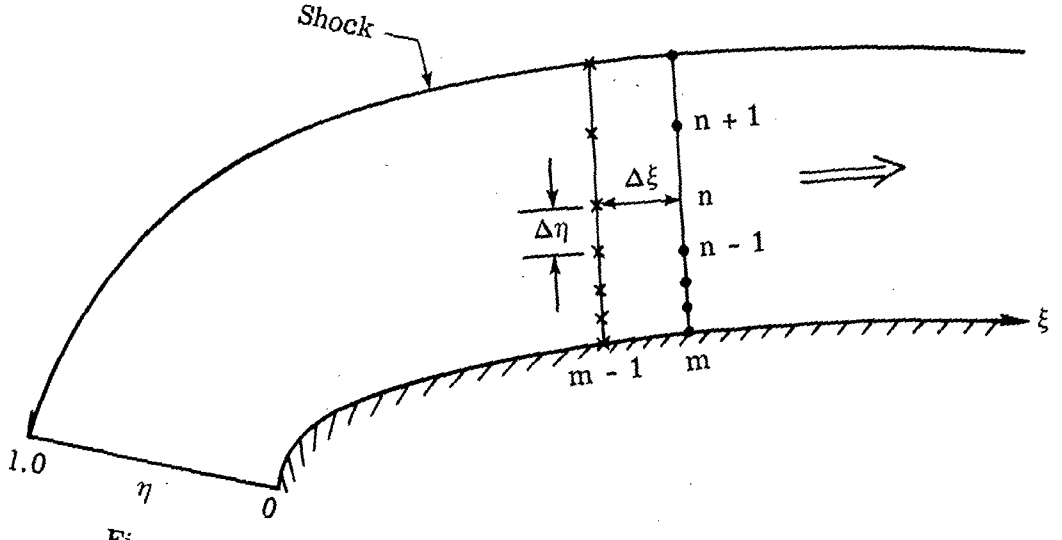

Figure 2.- Finite-difference representation of flow field.

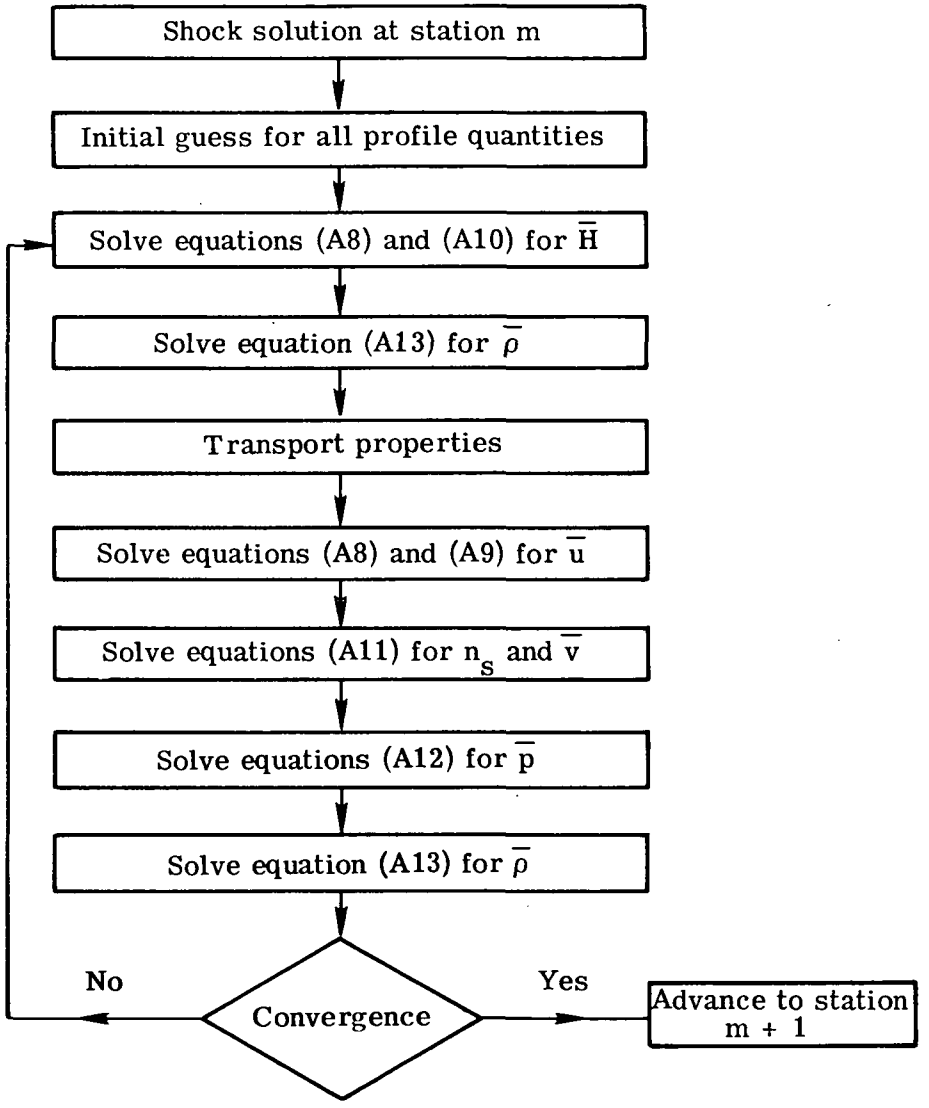

Figure 3.- Flow chart for solution sequence of viscous-shock-layer equations.

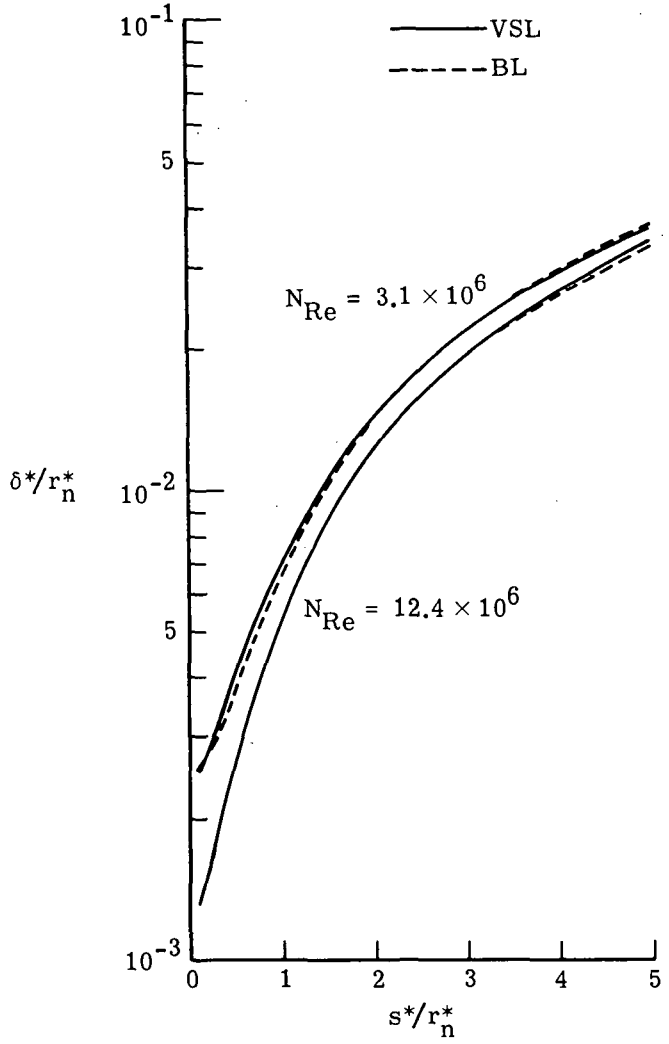

Figure 4.- Comparison of boundary-layer-thickness distributions.

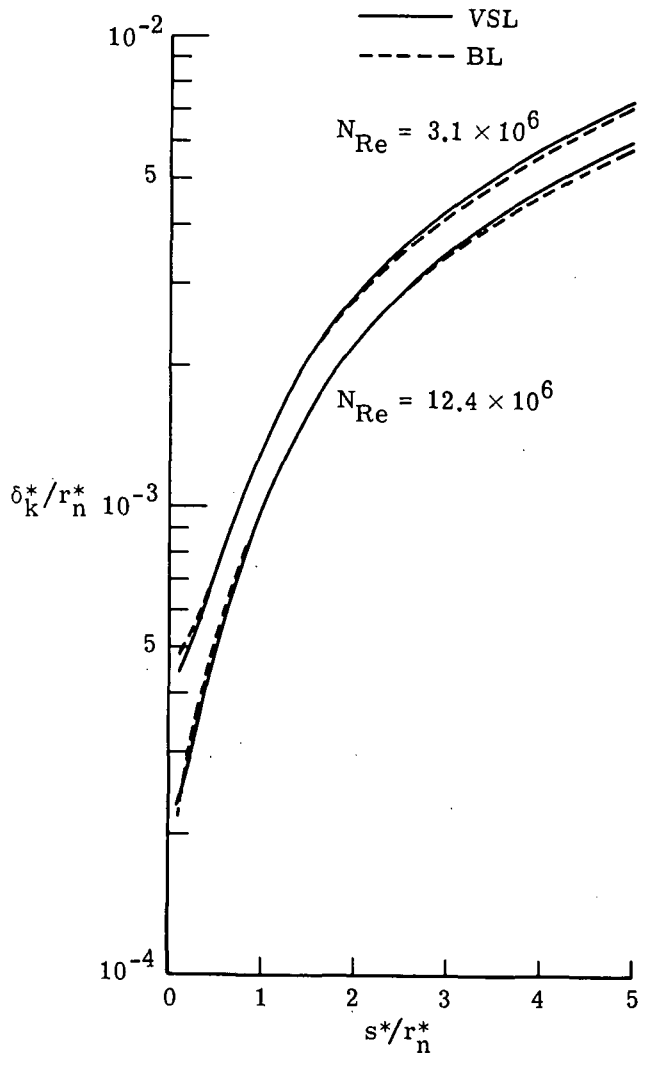

Figure 5.- Comparison of incompressible-displacement-thickness distributions.

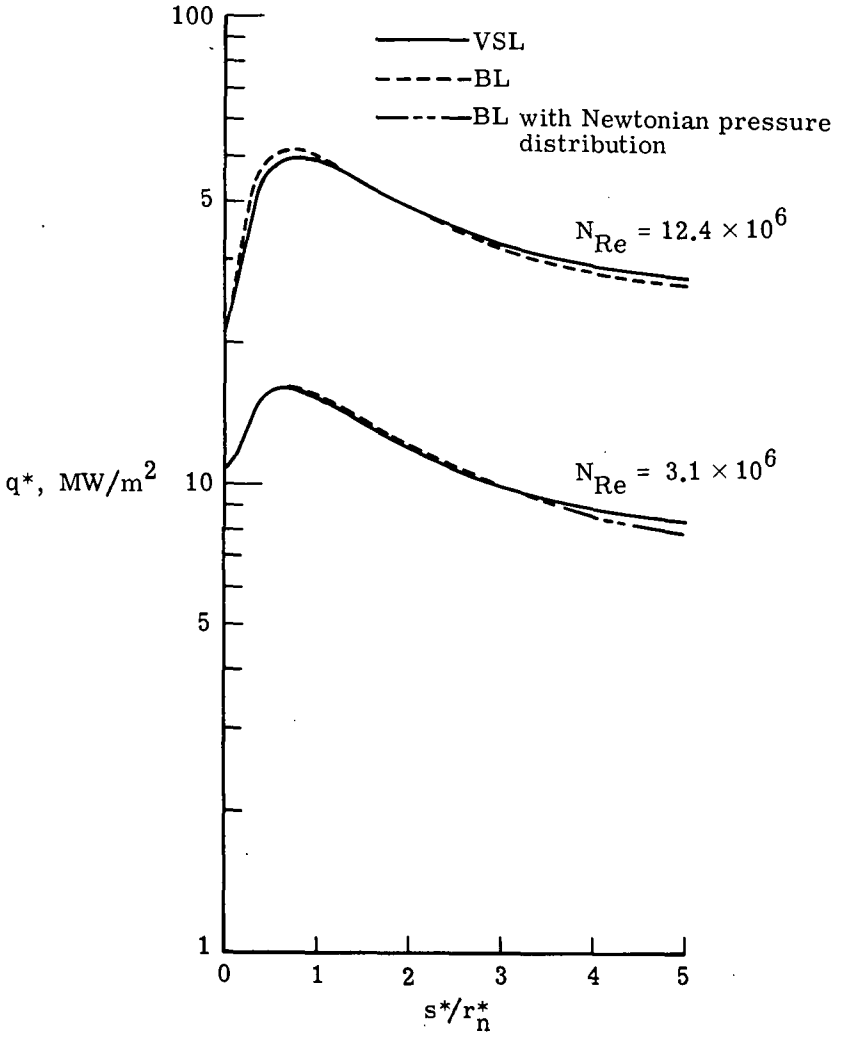

Figure 6.- Comparison of heat-transfer distributions.

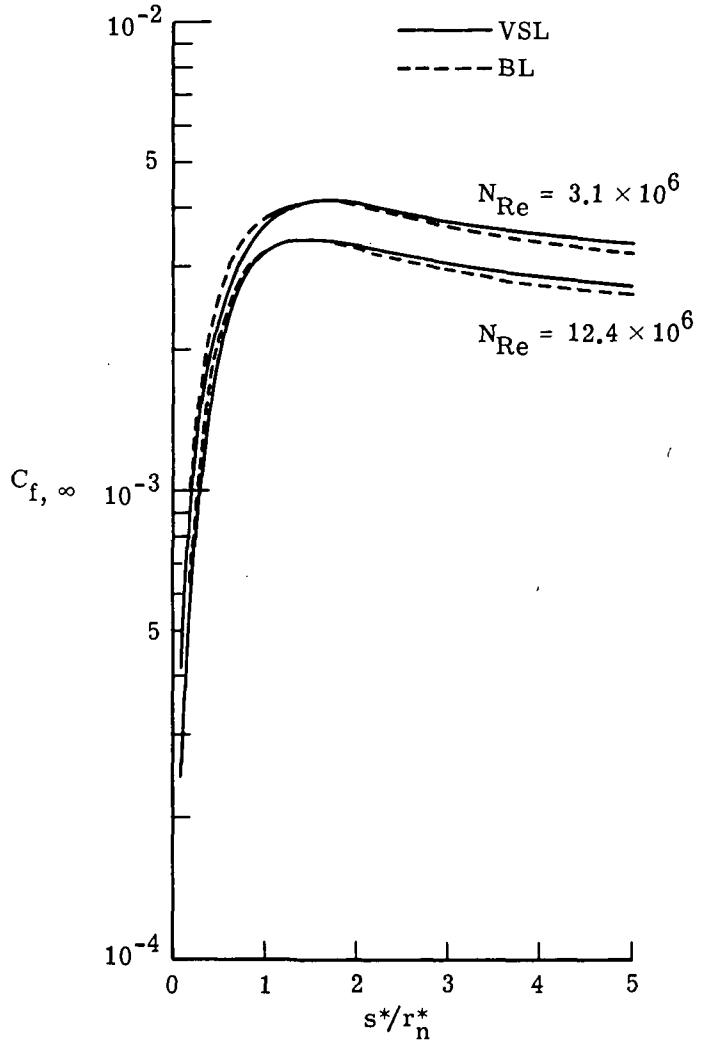

Figure 7.- Comparison of skin-friction distributions.

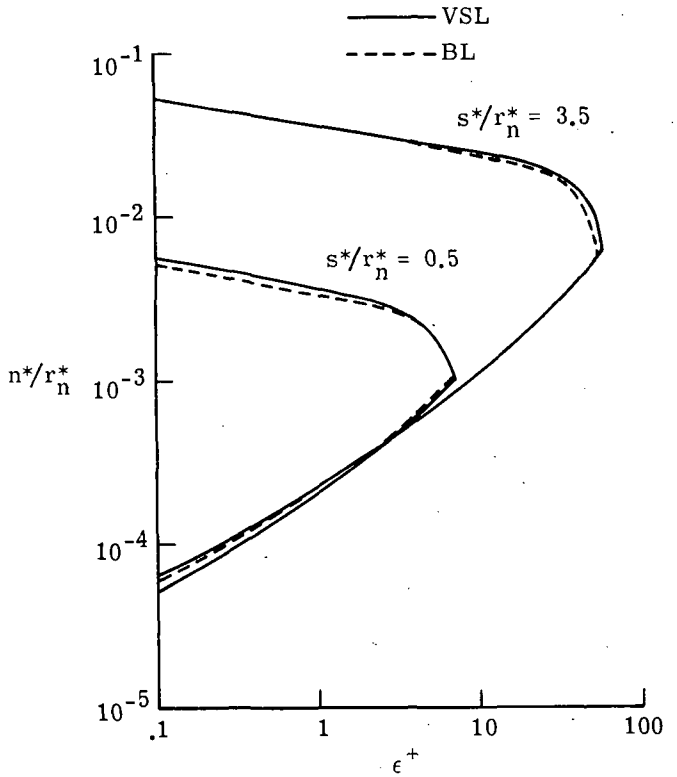

Figure 8.- Comparison of eddy-viscosity profiles. $N_{Re} = 3.1 \times 10^6$.

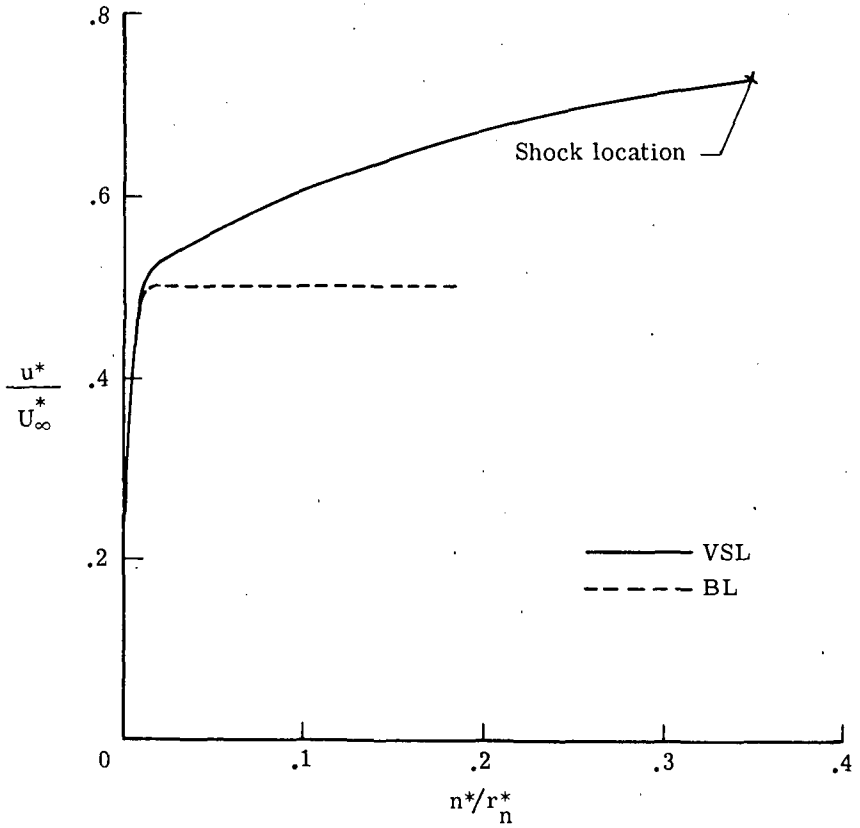

Figure 9.- Comparison of tangential velocity profiles at $s^*/r_n^* = 2.0$. $N_{Re} = 3.1 \times 10^6$.

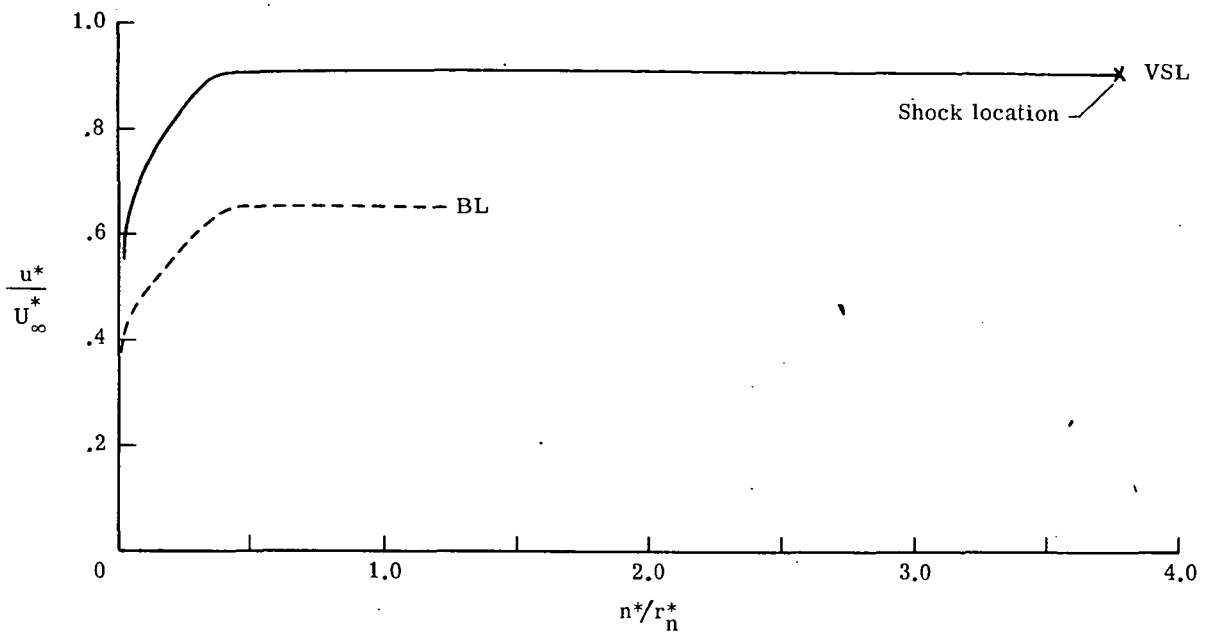

Figure 10.- Comparison of tangential velocity profiles at $s^*/r_n^* = 80$. $N_{Re} = 3.1 \times 10^6$.

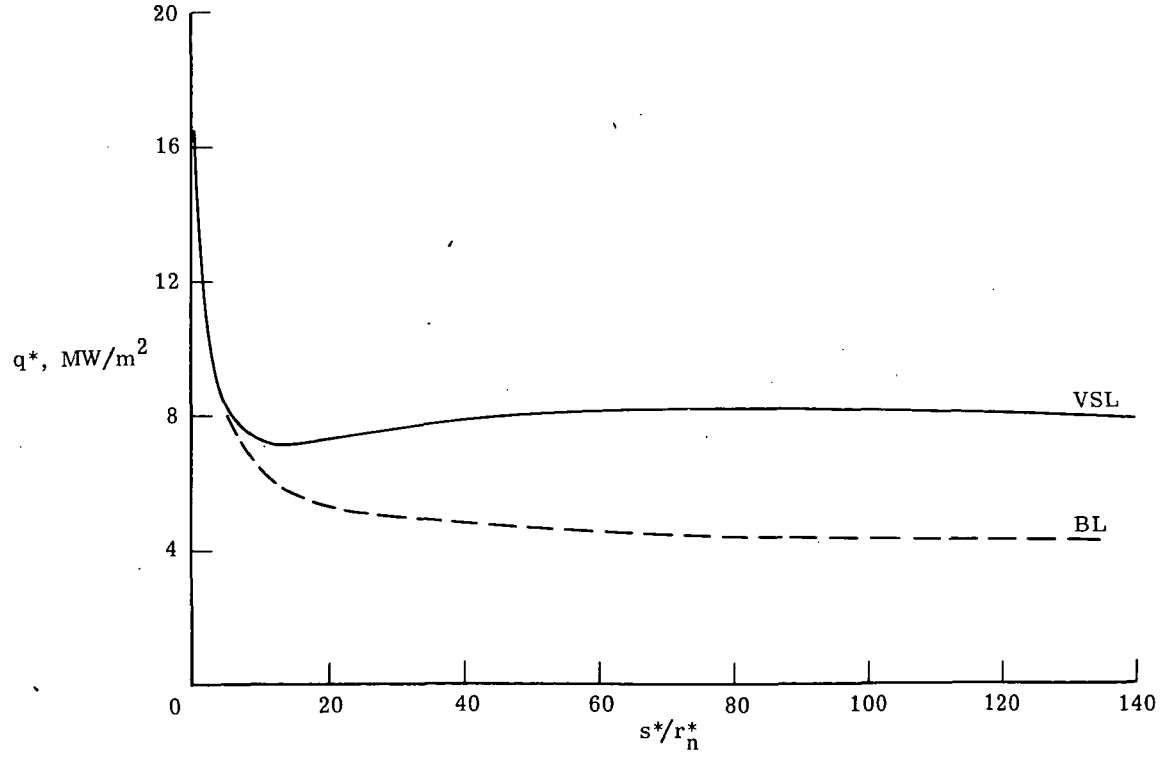

Figure 11.- Comparison of heat-transfer distributions. $N_{Re} = 3.1 \times 10^6$.

NATIONAL AERONAUTICS AND SPACE ADMINISTRATION
WASHINGTON, D.C. 20546

OFFICIAL BUSINESS
PENALTY FOR PRIVATE USE $300

SPECIAL FOURTH-CLASS RATE
BOOK

POSTAGE AND FEES PAID
NATIONAL AERONAUTICS AND
SPACE ADMINISTRATION
451

U.S.MAIL

223 001 C1 U AL 750207 S00120ES
PHILCO FORD CORP
AERONUTRONIC DIV
AEROSPACE & COMMUNICATIONS OPERATIONS
ATTN: TECHNICAL INFO SERVICES
JAMBOREE & FORD ROADS
NEWPORT BEACH CA 92663

POSTMASTER: If Undeliverable (Section 158 Postal Manual) Do Not Return

"The aeronautical and space activities of the United States shall be conducted so as to contribute . . . to the expansion of human knowledge of phenomena in the atmosphere and space. The Administration shall provide for the widest practicable and appropriate dissemination of information concerning its activities and the results thereof."

—NATIONAL AERONAUTICS AND SPACE ACT OF 1958

NASA SCIENTIFIC AND TECHNICAL PUBLICATIONS

TECHNICAL REPORTS: Scientific and technical information considered important, complete, and a lasting contribution to existing knowledge.

TECHNICAL NOTES: Information less broad in scope but nevertheless of importance as a contribution to existing knowledge.

TECHNICAL MEMORANDUMS: Information receiving limited distribution because of preliminary data, security classification, or other reasons. Also includes conference proceedings with either limited or unlimited distribution.

CONTRACTOR REPORTS: Scientific and technical information generated under a NASA contract or grant and considered an important contribution to existing knowledge.

TECHNICAL TRANSLATIONS: Information published in a foreign language considered to merit NASA distribution in English.

SPECIAL PUBLICATIONS: Information derived from or of value to NASA activities. Publications include final reports of major projects, monographs, data compilations, handbooks, sourcebooks, and special bibliographies.

TECHNOLOGY UTILIZATION PUBLICATIONS: Information on technology used by NASA that may be of particular interest in commercial and other non-aerospace applications. Publications include Tech Briefs, Technology Utilization Reports and Technology Surveys.

Details on the availability of these publications may be obtained from:

SCIENTIFIC AND TECHNICAL INFORMATION OFFICE

NATIONAL AERONAUTICS AND SPACE ADMINISTRATION

Washington, D.C. 20546